RESEARCH ARTICLE | JUNE 07 2024

Noise matching and sensitivity improvement in aluminum nitride nanoelectromechanical resonators via parametric amplification  $\bigcirc$ 

Tahmid Kaisar <sup>(1)</sup>; Philip X.-L. Feng **□** 



Appl. Phys. Lett. 124, 233511 (2024) https://doi.org/10.1063/5.0193395









## Noise matching and sensitivity improvement in aluminum nitride nanoelectromechanical resonators via parametric amplification

Cite as: Appl. Phys. Lett. 124, 233511 (2024); doi: 10.1063/5.0193395 Submitted: 21 December 2023 · Accepted: 26 April 2024 · Published Online: 7 June 2024







Tahmid Kaisar 🕞 and Philip X.-L. Feng<sup>a)</sup> 🕞



### **AFFILIATIONS**

Department of Electrical and Computer Engineering, Herbert Wertheim College of Engineering, University of Florida, Gainesville, Florida 32611, USA

a) Author to whom correspondence should be addressed: philip.feng@ufl.edu

#### **ABSTRACT**

Parametric amplification of ultrasmall signals from electromechanical transducers directly in the mechanical domain, prior to electrical readout, is an intriguing challenge and is important for both scientific measurements and technologies utilizing micro/nanoelectromechanical systems (MEMS/NEMS). Here, we report on parametric amplification of aluminum nitride (AlN) multimode NEMS resonators (with broad intrinsic dynamic ranges up to 90 dB) for enabling detection of their thermomechanical resonances in both optical and electrical readout schemes simultaneously. The experiments demonstrate that, upon parametric pumping, the electrically transduced thermomechanical motions experience significant amplification, surpassing the extrinsic electronic noise level, while still below the parametric pumping threshold. We achieve noise matching that enables room temperature force sensitivity of 0.46 fN/Hz<sup>1/2</sup>. We observe high parametric gain up to 650, accompanied by a strong boost (over 3.5 $\times$ ) in the effective quality factor ( $Q_{\text{eff}}$  from 9000 to 32 000). These findings underscore the utilities of parametric amplification in noise matching and improving force sensitivity for NEMS transducers and their emerging applications.

Published under an exclusive license by AIP Publishing. https://doi.org/10.1063/5.0193395

Parametric amplification has been widely employed in various fields, such as in optics, nanomechanics, and electronic circuits, to improve sensitivity of low-level signals through modulating system parameters. Because of achieving ultrahigh responsivities and sensitivities<sup>1,2</sup> at low power levels,<sup>2,3</sup> resonant nanoelectromechanical systems (NEMS) operating at high frequencies<sup>4</sup> are promising for resonant sensing<sup>1-3</sup> and high-precision measurements.<sup>5</sup> However, efficiency of their signal transduction is often limited by the noise floors of electronic amplifiers employed in the readout process, even by using cryogenic amplifiers having low noise figures.<sup>3,6</sup> Using parametric amplification, it is possible to amplify the signal directly in the mechanical domain first, before electrical transduction, thus evading or mitigating the adverse effects of amplifier noise. Parametric effects have been achieved in microelectromechanical systems (MEMS) and NEMS by modulating certain device parameters at twice the resonance frequency.<sup>7–11</sup> In addition to providing parametric gain, this approach has the potential to enhance the effective quality factor (Q<sub>eff</sub>) of a resonator,<sup>12</sup> improve the sensitivity of atomic force microscopy (AFM),<sup>13</sup> enhance the signal-to-noise-ratio (SNR) in gyroscopes, 14 reduce the

phase noise in parametric feedback oscillators, 15 and facilitate the creation of RF isolators.16

A number of experiments have recently been conducted to investigate the impact of parametric amplification in MEMS/NEMS.<sup>17</sup> Earlier, the first introduction of parametric amplification involved utilizing a 34 kHz microcantilever to achieve thermomechanical noise squeezing.<sup>25</sup> Subsequent investigations have yielded impressive results, such as a 25-fold enhancement of Qeff in piezoelectric GaAs/AlGaAs doubly clamped beam resonators<sup>26</sup> and a 1000-fold parametric gain with a 75-fold Q<sub>eff</sub> enhancement in GaAs beam resonators. <sup>10</sup> Similarly, silicon nitride (SiN) square membrane resonators have demonstrated a parametric gain of 100 and a 150-fold enhancement in Q<sub>eff</sub>.<sup>27</sup> In these studies,  $2\omega$  pumping is superposed on the driving signal (at  $\omega$ ), only utilizing a portion of parametric amplification range, and the undriven thermomechanical noise is not resolved. While detecting minuscule motions of NEMS transducers employing all-electronic transduction schemes, the undriven thermomechanical motion is often overwhelmed by the noise floors of the readout amplifiers, eventually causing noise mismatch, which has been a persistent problem in

NEMS displacement detection. In this Letter, we introduce parametric pumping to address this noise mismatching problem in piezoelectric aluminum nitride (AlN) square membrane NEMS resonators with broad intrinsic dynamic ranges (DRs) (up to 90 dB), where their intrinsic noise floors cannot readily be resolved in all-electronic transduction. We conduct parametric amplification experiments using both optical and piezoelectric readout schemes and observe that the undriven thermomechanical motion in piezoelectric transduction becomes observable below the parametric threshold (as calibrated in optical readout) of the NEMS transducer. Our investigation encompasses a comparative analysis of optical and electrical readout schemes, evaluating key parameters including dynamic range (DR), parametric gain, force sensitivity, and the enhancement of  $Q_{\rm eff}$  in piezoelectric multimode AlN NEMS resonators.

As most parametric MEMS/NEMS resonators reported to date have relied on varying the device stiffness, 7-27 we study AlN square membrane resonators (see S1 of the supplementary material for the fabrication process) where the stiffness can be efficiently modulated by varying the tension, thus facilitating parametric amplification. Resonant motion of AlN NEMS resonators under the effect of parametric amplification (pumping frequency,  $f_{\text{pump},n} = 2f_n$ , where  $f_n$  is the resonance mode of interest) can be written as

$$m\ddot{x} + \frac{m\omega_0\dot{x}}{Q} + [k_1 + k_p\cos(2\omega_0t)]x + k_3x^3 = F(t).$$
 (1)

Here,  $k_{\rm p}{\rm cos}(2\omega_0 t)$  is the periodic modulation of linear spring constant (stiffness) at  $2\omega_0$ , and  $k_{\rm p}$  is the pumping strength, m,  $\omega_0$ ,  $k_1$ ,  $k_3$ , and F(t) are the effective mass, angular resonance frequency of fundamental mode, linear spring constant, Duffing coefficient, and driving force, respectively. When there is no external driving force, F(t) corresponds to the Langevin force originating from thermomechanical fluctuations, which lead to the undriven thermomechanical motion that sets the intrinsic noise floor of the resonator.

Figure 1 displays the overview of this work with illustrations of DR, Duffing nonlinearity, parametric amplification of undriven thermomechanical noise and its effect to resolve noise mismatching. The signal transduction diagram of a generalized measurement scheme with two cascaded stages is demonstrated in Fig. 1(a), which shows a noise-free transducer (NEMS) with a front-end amplifier. The input signal x(t) to the transducer is a sinusoidal waveform describing the device motion in the displacement domain, accompanied by the thermomechanical motion of the device. The transducer converts the displacement-domain signal to voltage-domain signal v(t) with a responsivity of  $\Re_{\text{elec}} = \partial v/\partial x$ . In the second stage of the transduction, the voltage-domain signal is multiplied with the gain (G) of the front-end low-noise amplifier (LNA), with thermal and flicker (1/f) noise added from the amplifier [Fig. 1(a)]. Figures 1(c) and 1(d) illustrate the fundamental definition of DR of a transducer or amplifier where DR is defined as the ratio between the 1 dB compression point (signal ceiling) and the minimum detectable signal (noise floor). Figure 1(e) demonstrates the cascaded DR of two stages of the transduction scheme. In a cascaded system, the system DR is determined by the least optimal stage (transducer with the narrowest DR), i.e.,  $DR_{sys} \leq min(DR_{i=1,N})$ . The intrinsic thermomechanical fluctuations of the first stage NEMS transducer is often lower than the noise floor of the front-end amplifier, leading to noise mismatch at the readout stage, thereby compromising the system's sensitivity and usable DR [Fig. 1(f)]. This limitation imposes practical implications on the transducer's performance. The solution to this problem is demonstrated in Figs. 1(b) and 1(g), where a parametric  $(2\omega)$  pump signal is applied to amplify the signal initially in the mechanical (displacement) domain before employing electronic amplification. Due to parametric pumping, the thermomechanical resonance spectral linewidth gets narrower, and the resonance peak emerges above the noise floor of the LNA, thus the noise matching is achieved, where the device intrinsic noise power (thermomechanical noise resonance) equals the extrinsic noise power (LNA noise floor).

Figure 2(a) shows a two-port electrical transduction scheme where a network analyzer is used to measure the driven resonance (at f), and a suitable LNA (Femto HVA-200M-40B) is used to amplify the AlN NEMS resonance signal. We use 20 dB gain of this LNA for all the electrical measurements in this study, and all the measured results are referred to the input (RTI) of the LNA. Optical transduction using laser interferometry measurement<sup>31</sup> is shown in Fig. 2(b), where a 785 nm diode laser is used to detect the resonance motion. An optical neutral-density (ND) filter is used to attenuate laser power, and a photodetector (PD) is used to convert the optical signal into electronic signal. Parametric pumping (at 2ω) is applied using a function generator, and the undriven thermomechanical noise spectrum is recorded using a spectrum analyzer. Figures 2(c) and 2(d) and Figs. 2(f) and 2(g) demonstrate the fundamental mode (~7 MHz) driven resonances in the AlN NEMS resonators (devices A and B) in electrical and optical transduction, respectively. Electrically and optically measured driven resonances of the second and third modes of device B are shown in Figs. 2(e) and 2(h). All measurements are done at room temperature in moderate vacuum  $(\sim 20 \, \mathrm{mTorr})$ .

Duffing nonlinearity, thermomechanical noise, DR, and parametric effects of device A are first characterized and displayed in Fig. 3. The displacement-domain thermomechanical noise spectral density on resonance,  $S_{x,\text{th}}^{1/2} \approx 0.11\,\text{pm/Hz}^{1/2}$ , is calculated based on a damped (finite-Q) simple harmonic resonator model, <sup>31</sup>

$$S_{x,\text{th}}^{1/2}(\omega) = \left[ \frac{4\,\omega_0\,k_{\rm B}\,T}{Q\,m} \frac{1}{\left(\omega_0^2 - \omega^2\right)^2 + \left(\frac{\omega\,\omega_0}{Q}\right)^2} \right]^{1/2}.\tag{2}$$

Here, in Eq. (2),  $k_{\rm B}$  and T are the Boltzmann's constant and temperature. The voltage-domain noise spectral density is  $S_{\nu,{\rm th}}^{1/2}=(S_{\nu,{\rm total}}-S_{\nu,{\rm sys}})^{1/2}\approx 0.14\,\mu{\rm V/Hz^{1/2}}$ , where  $S_{\nu,{\rm sys}}$  is the voltage-domain noise floor (noise power level) of the measurement system. The displacement responsivity of the optical readout system is  $\Re_{\rm opt}=S_{\nu,{\rm th}}^{1/2}/S_{x,{\rm th}}^{1/2}\approx 1.20\,\mu{\rm V/pm}$ . Using this responsivity expression of optical and electrical transduction (see Sec. S2 in the supplementary material), the voltage-domain signals are converted into displacement-domain signals. We further drive the NEMS resonator into the nonlinear regime by increasing RF excitation in both optical and electrical measurement schemes to calculate the DR [Figs. 3(a)–3(b)]. The critical displacement of a square membrane resonator can be estimated by.

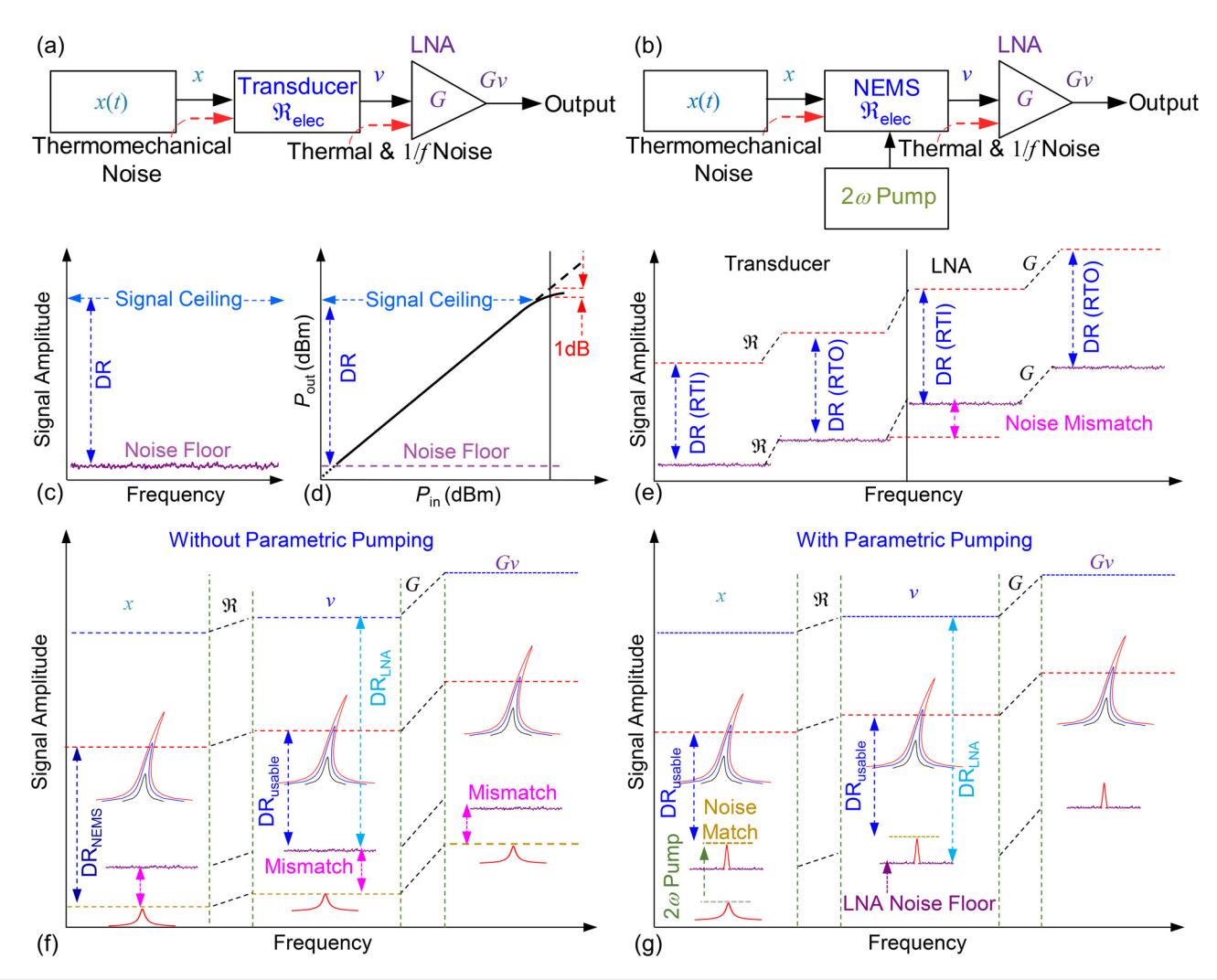


FIG. 1. Conceptual illustration of noise mismatching problem and solution for NEMS transducers in piezoelectric transduction. (a) Signal transduction diagram of a basic measurement scheme with a front-end low-noise amplifier (LNA). (b) Signal transduction diagram of a NEMS transducer with 2ω pump, followed by a LNA. (c) and (d) Illustrations of dynamic range (DR) in signal amplitude, and in output vs input signal power. (e) Noise mismatch in a cascaded measurement system where the amplifier's noise floor is higher than the transducer's noise floor. RTI(O) stands for referred to input (output). (f) Illustration of Duffing nonlinearity, DR, and noise mismatch problem of a NEMS transducer without parametric pumping in each transduction stage. DR<sub>NEMS</sub> is the intrinsic DR of the NEMS transducer measured in optical readout, and DR<sub>usable</sub> is the usable DR of NEMS measured in the electrical readout. DR<sub>LNA</sub> is measured in the voltage domain [v(t)] at the input of the LNA. Both DR<sub>LNA</sub> and DR<sub>usable</sub> are transduced to the displacement domain [x(t)] using the responsivity of the NEMS transducer in piezoelectric transduction. (g) Solution to the noise mismatching problem by applying parametric pumping.

$$a_{\text{c,peak}} = \sqrt{2}a_{\text{c,rms}} = \left(\frac{32\pi^2 m f_0^2}{3\sqrt{3}Qk_3}\right)^{1/2}.$$
 (3)

From the onset of nonlinearity (1 dB compression point) and thermomechanical noise of the device, the  $DR_{NEMS}$  is determined as  $^{32}$ 

$$DR_{NEMS} = 20log \left[ \frac{0.745 a_{c,rms}}{S_{x,th}^{1/2} BW^{1/2}} \right], \tag{4}$$

where often  $BW=1\,\mathrm{Hz}$  is the measurement bandwidth. From Eq. (4), we calculate the DR<sub>NEMS</sub>  $\approx$  80 dB from the optically measured data,

which is in good agreement with the theoretical  $DR_{NEMS,theory}\!=\!86\,dB.$  In electrical measurement, the usable DR of the NEMS transducer,  $DR_{usable}\!\approx\!48\,dB$ , is defined as the ratio of the electrically measured onset of nonlinearity of the NEMS transducer and the electrical noise floor.

We then characterize the parametric pumping effects of thermomechanical noise in this device using both optical and electrical readout schemes with resolution bandwidth (RBW) of 510 Hz. First, in optical readout, we apply highly efficient electrical parametric pump to the resonator from  $\nu_p = 1$  to 30 mV, which shows clear signatures of parametric amplification. The displacement-domain noise spectral density of a parametrically pumped resonator is  $^{22,33}$ 

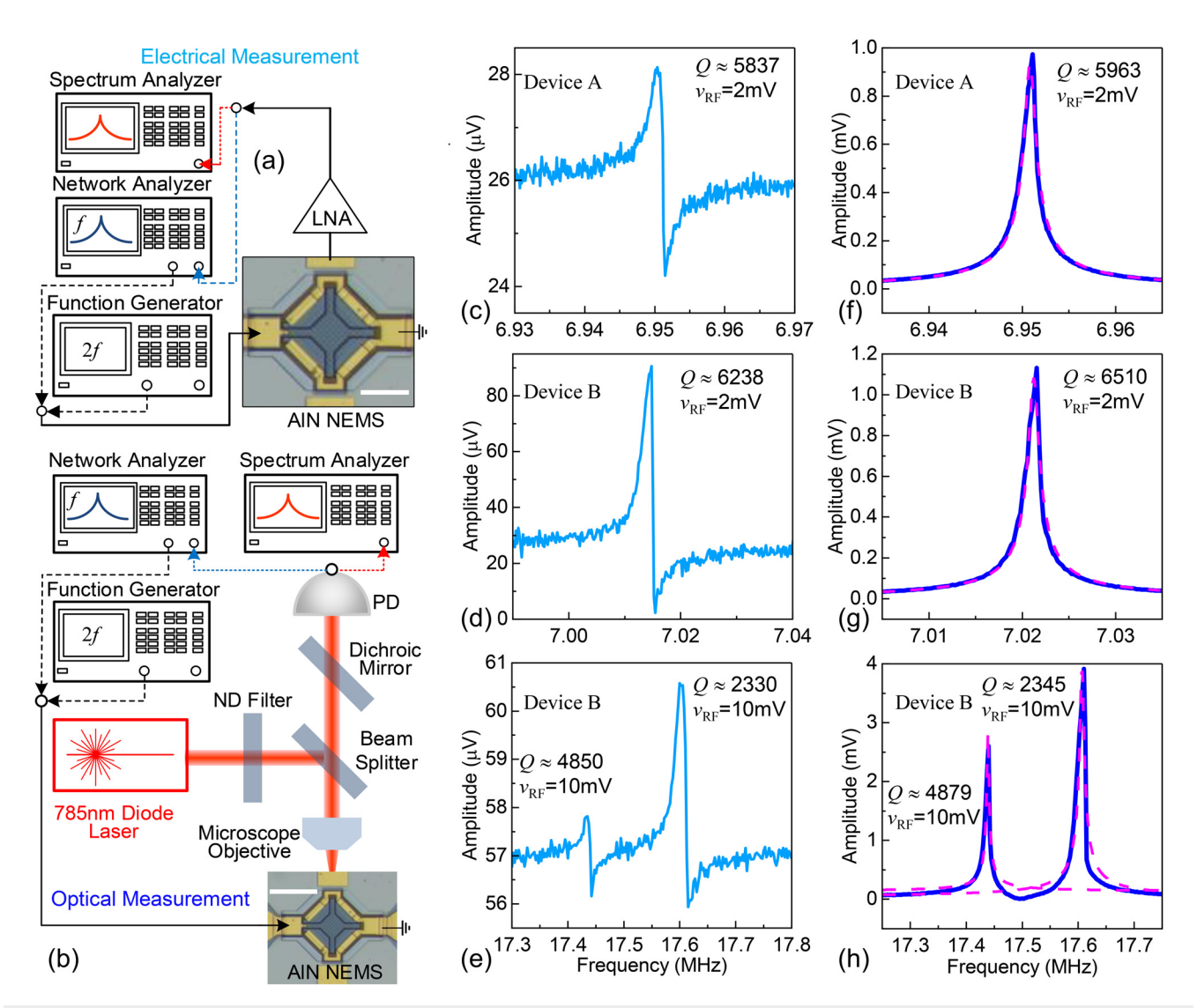


FIG. 2. Schematic illustration of the measurement systems with measured driven resonances in both optical and electrical readout schemes: (a) electrical measurement scheme and (b) optical measurement scheme. Scale bars in the optical micrographs of devices: 20 μm. Electrically measured, electrically driven resonances with their Q factors: (c) first mode of device A, (d) first mode of device B, (e) second and third modes of device B. Optically measured, electrically driven resonances with their Q factors: (f) first mode of device A, (g) first mode of device B, and (h) second and third modes of device B. The magenta dashed lines are fitting curves to the damped (finite-Q) harmonic resonator model.

$$S_{x,\text{th,pump}}^{1/2}(\omega) = \sqrt{\frac{k_B T \left(\frac{\omega_0^2}{4Q^2} + (\omega - \omega_0)^2 + \frac{1}{4} \frac{v_p^2}{v_t^2} \frac{\omega_0^2}{Q^2}\right)}{m\omega_0 Q \left[(\omega - \omega_0)^4 + 2(\omega - \omega_0)^2 \left(\frac{1}{4} \frac{\omega_0^2}{Q^2} + \frac{1}{4} \frac{v_p^2}{v_t^2} \frac{\omega_0^2}{Q^2}\right) + \left(\frac{1}{4} \frac{\omega_0^2}{Q^2} - \frac{1}{4} \frac{v_p^2}{v_t^2} \frac{\omega_0^2}{Q^2}\right)^2\right]}},$$
(5)

where  $v_t$  is the parametric threshold voltage. The measured parametric gain of thermomechanical noise in optical readout can be calculated

from Fig. 3(c). In the range of  $\nu_p < \nu_b$  the parametric gain below the threshold can be expressed as  $^{33}$ 

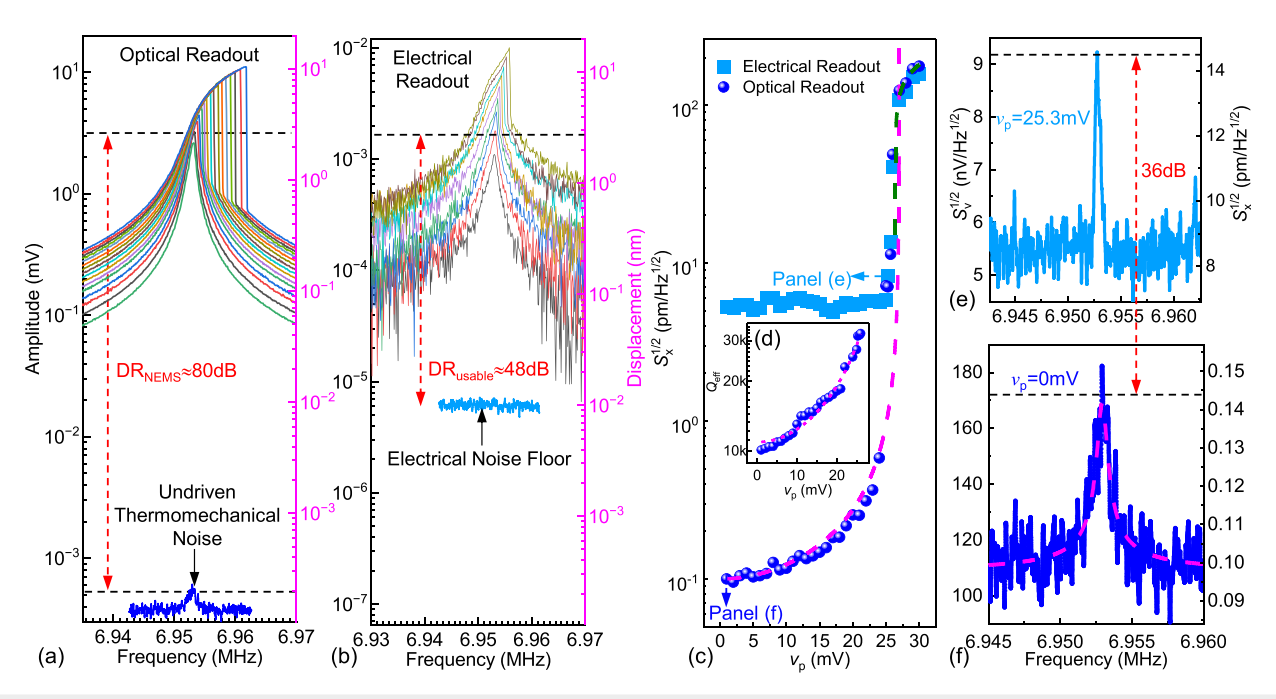


FIG. 3. Parametric amplification and noise matching in the fundamental mode of an AIN NEMS resonator (device A). (a) Thermomechanical noise and driven resonances with varying  $v_{RF} = 0.8$  to 3.8 mV with 0.2 mV step to characterize DR in the optical readout. (b) Driven resonances (after background subtraction) with varying  $v_{RF} = 0.8$  to 4.2 mV to characterize DR in electrical transduction. (c) Comparison between data from optical and electrical readout schemes in displacement domain with inset (d) showing  $Q_{eff}$  enhancement in optical transduction for  $v_p = 1$  to 30 mV. Magenta and olive dashed lines show the fitting to Eqs. (6) and (7). (e) Thermomechanical noise measured in piezoelectric transduction at noise matching condition ( $v_p = 25.3$  mV). (f) Thermomechanical noise measured in optical transduction without parametric pumping ( $v_p = 0$  mV), with magenta dashed line being the fitting curve to the finite-Q harmonic resonator model [Eq. (2)], yielding  $Q \approx 9000$ .

$$G = \sqrt{1 + \left(\frac{\nu_p}{\nu_t}\right)^2} / \left[1 - \left(\frac{\nu_p}{\nu_t}\right)^2\right]. \tag{6}$$

As  $v_{\rm p}$  approaches  $v_{\rm b}$  Eq. (6) diverges; as a result, higher parametric gain and enhancement of  $Q_{\rm eff}$  are observed [Figs. 3(c) and 3(d)]. In the range of  $v_{\rm p} > v_{\rm b}$  the device goes to self-oscillation regime, and the displacement saturates because of Duffing nonlinearity and nonlinear damping. In this  $v_{\rm p} > v_{\rm t}$  region, the parametric gain is determined by the ratio of Duffing limited parametrically amplified displacement and the thermomechanical noise floor as  $^{22}$ 

$$G = \sqrt{\frac{m^2 \omega_0^5 \sqrt{\left(\frac{\nu_{\rm p}}{\nu_{\rm t}}\right)^2 - 1}}{3k_{\rm B} T Q^2 |k_3|}}.$$
 (7)

By performing curve fitting using the model based on Eqs. (5)–(7), we find the parametric threshold  $\nu_{\rm t}\approx 26.4\,{\rm mV}$  for the fundamental mode of device A. In the region of  $\nu_{\rm p}<\nu_{\rm b}$  the measured parametric gain is up to  $G=S_{x,{\rm th,pump}}^{1/2}(\omega_0)/S_{x,{\rm th}}^{1/2}(\omega_0)\approx 650$ . The critical parametric gain  $^{22}$  (where the olive dashed line diverges from the magenta dashed line) for device A is found to be  $G_{\rm crt}\approx 1000$ .

We also demonstrate spectral linewidth narrowing due to parametric pumping which eventually results in an increase in  $Q_{\rm eff}$ . In the  $\nu_p < \nu_t$  region,  $Q_{\rm eff}$  is defined as  $^{22}$ 

$$Q_{\text{eff}} = Q \frac{\left(\nu_{p}^{2} + \nu_{t}^{2}\right)\nu_{t}}{\sqrt{\left(\nu_{p}^{2} + \nu_{t}^{2}\right)\left(\sqrt{\nu_{p}^{8} + 14\nu_{p}^{4}\nu_{t}^{4} + \nu_{t}^{8} - 4\nu_{p}^{2}\nu_{t}^{2}}\right)}}.$$
 (8)

The undriven thermomechanical resonance shows a  $Q \approx 9000$ without parametric pumping ( $v_p = 0 \text{ mV}$ ). After fitting our measured data with Eq. (8), we obtain  $Q_{\text{eff}} \approx 32\,000$  below threshold, which is over  $\sim 3.5 \times$  booster of Q [Fig. 3(d)]. Finally, we compare the parametric amplification of thermomechanical noise between optical and piezoelectric readout schemes [Fig. 3(c)] in displacement domain, as the displacement of the resonator due to undriven thermomechanical motion is the same in both optical and piezoelectric measurements after a certain  $v_p$  where the thermomechanical noise can be detected in piezoelectric transduction. As a result, we calculate the responsivity in piezoelectric transduction as  $\Re_{\rm elec} = S_{\nu, {\rm elec}}^{1/2} / S_{x, {\rm opt}}^{1/2} \approx 0.62 \, \mu {\rm V/nm}$ , where  $S_{\nu, {\rm elec}}^{1/2}$  and  $S_{x, {\rm opt}}^{1/2}$  are the voltage-domain thermomechanical noise in piezoelectric transduction and displacement-domain thermomechanical noise in optical transduction, respectively, measured after parametric pumping threshold. In electrical transduction, noise from the measurement system is higher than the piezoelectrically transduced thermomechanical noise; thus, it cannot be seen as the signal is overwhelmed by the system noise floor. After applying parametrical pumping, electrically transduced thermomechanical noise emerges above the noise floor of the amplifier at  $v_p \approx 25.3 \, \text{mV}$  [Fig. 3(e)], which is still below the parametric threshold ( $v_t \approx 26.4 \,\mathrm{mV}$ ) calibrated in optical

transduction. Above this  $v_{\rm p}\approx 25.3\,{\rm mV}$  point, we achieve noise matching, and the ratio of thermomechanical resonance peak to electrical noise floor is enhanced by  $\approx 100\,\times$ . At this noise matching condition, we obtain a force sensitivity  $^{25,34}$   $S_F^{1/2}=\sqrt{\frac{4k_{\rm B}Tm\omega_0}{Q_{\rm eff}}}=0.46\,{\rm fN/Hz^{1/2}}$  (where  $Q_{\rm eff}\approx 31\,750$  at the noise matching condition) limited by thermomechanical noise, which otherwise cannot be achieved without parametric pumping in piezoelectric transduction. Based on the comparison between the parametric pumping in the optical and electrical domains, we determine that although the piezoelectrically transduced thermomechanical noise is  $\approx 36\,{\rm dB}$  lower than the noise floor of the measurement system, the parametric pumping can greatly amplify the signal while maintaining noise level of the system, allowing to characterize the weak electrical signal from the device

We further explore the Duffing nonlinearity and parametric amplification of thermomechanical noise in another AlN NEMS resonator (device B). Without parametric pumping, the thermomechanical noise spectrum of device B shows a fundamental resonance at  $\approx 7.02$  MHz with  $Q\approx 8500$  [Figs. 4(a) and 4(f)]. We increase  $\nu_{RF}$  from 0.8 to 3.8 mV and observe a stiffening Duffing nonlinearity. The transduction responsivity of the optical interferometry is  $\Re_{\rm opt}\approx 1.80~\mu{\rm V/pm}$  for this device. By taking the ratio between the onset of nonlinearity and the thermomechanical noise floor, we obtain a DR\_NEMS  $\approx 78~{\rm dB}$  for the fundamental mode. We then apply  $\nu_{\rm p}=1$  to 26 mV in both optical and electrical measurement schemes. In optical measurement, we find  $\nu_{\rm t}\approx 24.1~{\rm mV}$  by fitting of Eqs. (5)–(7). We observe a parametric gain  $G\approx 584$  and critical gain  $G_{\rm crt}\approx 614$  [Fig. 4(b)]. We also achieve a boosted  $Q_{\rm eff}\approx 30\,000$  below the threshold pump.

The responsivity of this device for the electrical measurement,  $\Re_{\rm elec}=0.74\,\mu{\rm V/nm},$  is calculated via the same method as for device A. Thermomechanical motion in this piezoelectric transduction emerges above the noise floor of the LNA at  $\nu_{\rm p}=23.5\,{\rm mV}$  [Fig. 4(e)]. At this noise matching point, we obtain a force sensitivity of  $S_F^{1/2}=0.69\,{\rm fN/Hz^{1/2}}$  and a  $70\times$  enhancement in the ratio of thermomechanical resonance peak to the electrical noise floor.

We also study parametric effects of thermomechanical noise in the third mode (17.5 MHz) of device B having  $Q \approx 5000$ . Duffing nonlinearity and DR of this mode are also characterized [Fig. 5(a)]. The responsivity and DR in optical readout are calculated as  $\Re_{\rm opt} \approx 3.71 \, \rm nV/fm = 3.71 \, \mu V/pm$  and  $\rm DR_{NEMS} \approx 90 \, dB$ , respectively. We then vary  $v_p = 1$  to 55 mV in both optical and electrical readout schemes. For this mode, all measurements are performed using RBW of 3 kHz. We obtain  $v_t \approx 51.8 \,\mathrm{mV}$ ,  $G \approx 70$ , and  $G_{\rm crt} \approx 86 \,\mathrm{[Fig. 5(b)]}$ by fitting Eqs. (5)–(7).  $Q_{\text{eff}} \approx 12\,000$  is found before the device goes into self-oscillation regime [Fig. 5(c)]. This mode shows a higher  $v_t$ compared to the fundamental mode as the third mode has higher  $k_1$ and lower Q compared to the first mode, which results in a larger  $k_t$ where  $k_t = 2k_1/Q^{\frac{7}{10}}$  While comparing between electrical and optical measurements with increasing  $v_p$  [Fig. 5(d)], we find that thermomechanical noise in piezoelectric transduction is seen above the noise floor of the LNA (noise matching condition) at  $v_p = 49.7 \,\mathrm{mV}$ [Fig. 5(e)], lower than  $v_t \approx 52.3$  mV for this mode. The responsivity in this piezoelectric transduction is calculated to be  $\Re_{\text{elec}} = S_{\nu,\text{elec}}^{1/2}/S_{x,\text{opt}}^{1/2}$  $\approx$  13.6  $\mu$ V/nm. Satisfying the noise matching condition by parametric pumping for this mode enables us to achieve a force sensitivity of  $^2 = 1.6 \text{ fN/Hz}^{1/2}$ . Measured main parametric amplification characteristics are summarized in Table I.

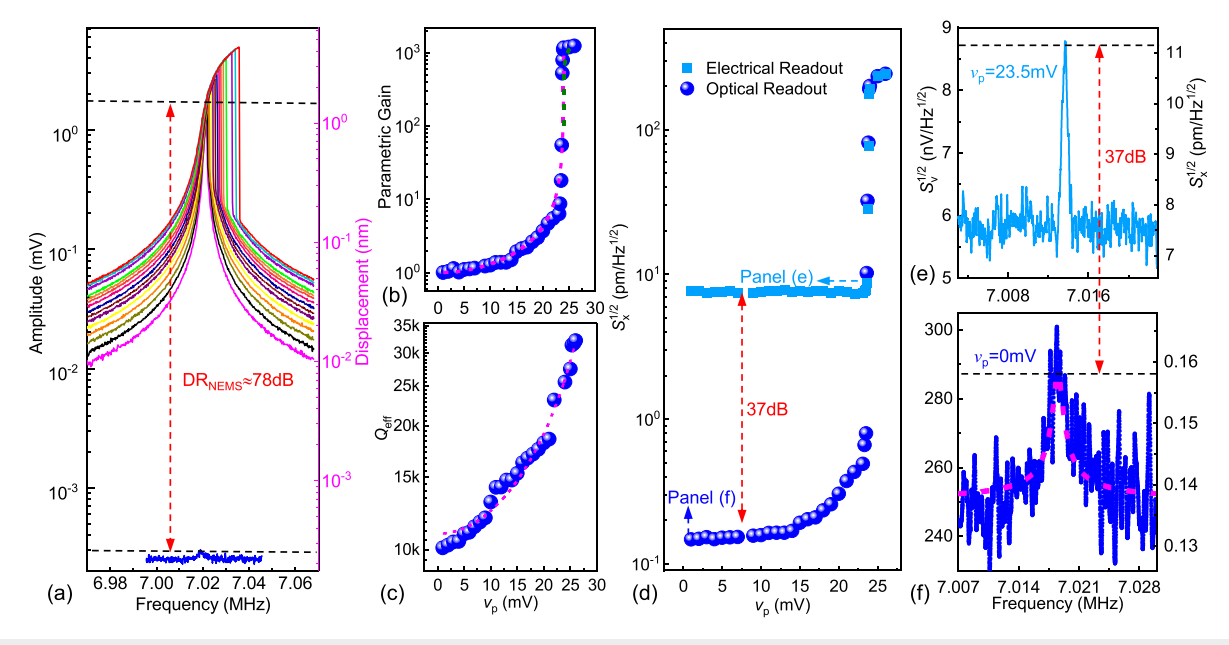


**FIG. 4.** Parametric amplification and noise matching in the fundamental mode of an AIN NEMS resonator (device B). (a) Thermomechanical noise and driven resonances with varying  $v_{RF} = 0.8$  to 3.8 mV with 0.2 mV step to characterize DR in the optical readout. (b) and (c) Parametric gain and  $Q_{eff}$  enhancement in optical transduction with  $v_p = 1$  to 26 mV. Magenta and olive dashed lines show the fitting to Eqs. (6) and (7). (d) Comparison between optical and electrical readout data in displacement domain. (e) Thermomechanical noise measured in piezoelectric transduction at noise matching condition ( $v_p = 23.5$  mV). (f) Thermomechanical noise in optical transduction without parametric pumping ( $v_p = 0$  mV), with magenta dashed line being the fitting curve to the finite-Q harmonic resonator model [Eq. (2)], giving  $Q \approx 8500$ .

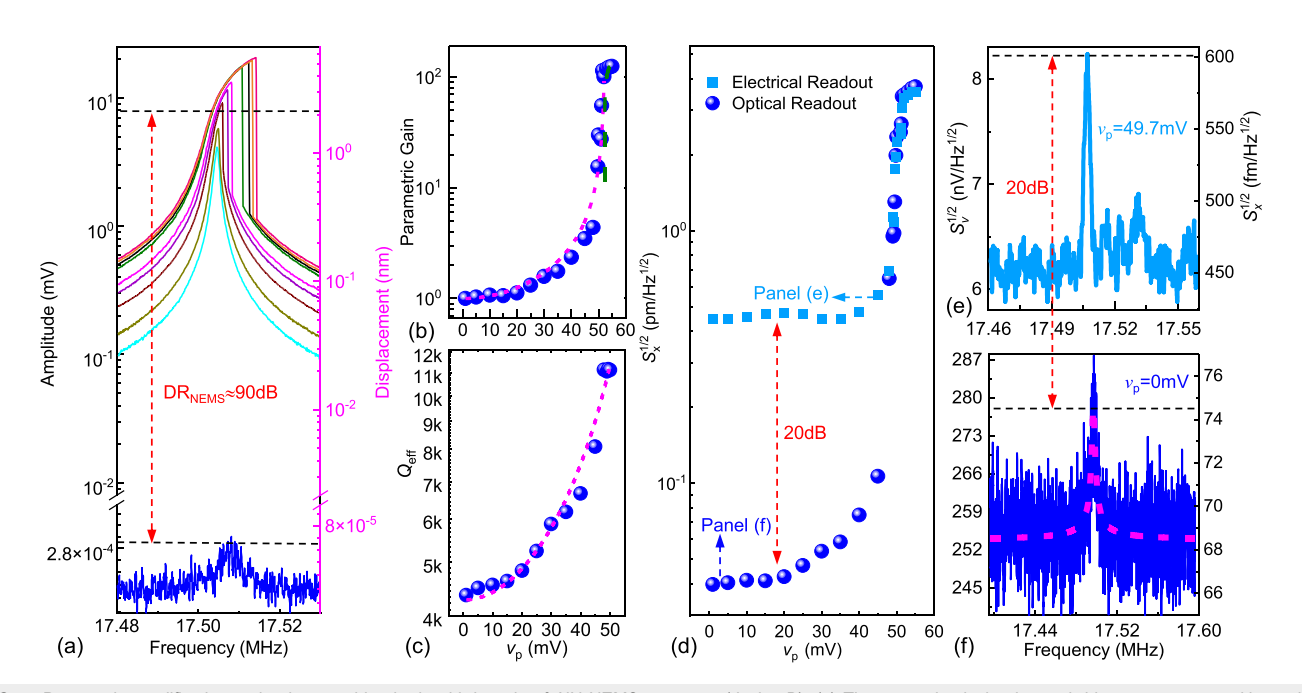


FIG. 5. Parametric amplification and noise matching in the third mode of AIN NEMS resonator (device B). (a) Thermomechanical noise and driven resonances with varying  $v_{RF}=10$  to 18 mV with 1 mV step to characterize DR in optical readout. (b) and (c) Parametric gain and  $Q_{eff}$  enhancement in optical transduction with  $v_p=1$  to 55 mV. Magenta and olive dashed lines show the fitting to Eqs. (6) and (7). (d) Comparison between data measured from optical and electrical readout schemes in displacement domain. (e) Thermomechanical noise measured in piezoelectric transduction at noise matching condition ( $v_p \approx 49.7$  mV). (f) Thermomechanical noise in optical transduction without parametric pumping ( $v_p=0$  mV), with magenta dashed line curve showing the fitting to the finite-Q harmonic resonator model [Eq. (2)], yielding  $Q\approx 5000$ .

 TABLE I. Summary of parametric amplification and noise matching characteristics.

Device ID	A	В	
Mode #	First	First	Third
Frequency $f_0$ (MHz)	6.95	7.02	17.6
Thermomechanical resonance	9000	8500	5000
Q (optical readout)			
Highest measured Q <sub>eff</sub>	32 000	30 000	12 000
with parametric pumping			
Measured device intrinsic DR (dB)	80	78	90
Parametric amplification gain, G	650	584	70
$v_p$ at noise matching condition (mV)	25.3	23.5	49.7
Threshold pump voltage $v_t$ (mV)	26.4	24.1	52.3
Force sensitivity $S_F^{1/2}$ (fN/Hz <sup>1/2</sup> )	0.46	0.69	1.60

In conclusion, we have demonstrated parametric amplification of thermomechanical motions in multimode AlN square membrane NEMS resonators employing both optical and electrical readout schemes. We have achieved parametric gain of 650 and over 3.5× enhancement in  $Q_{\rm eff}$  for the fundamental mode (device A), while for the third mode (device B), we have obtained parametric gain of 70 and 2.7× enhancement in  $Q_{\rm eff}$ . We have achieved noise matching condition below the parametric threshold of the NEMS transducer (repeatedly across different devices and different modes), resulting in a fundamental-mode force sensitivity of 0.46 fN/Hz<sup>1/2</sup> at room

temperature. These findings offer valuable insights for realizing NEMS parametric amplifiers with ideal mechanical gain and thermomechanical noise matching in high-precision all-electronic measurements.

See the supplementary material for the following details: fabrication of AlN square membrane NEMS resonators, parametric pumping of the 1st mode of device A, parametric pumping of the 1st mode of device B, parametric pumping of the 3rd mode of device B, parametric instability tongue of the 1st mode of device A, quality factor extraction from driven resonance in electrical readout, intrinsic dynamic range and usable dynamic range of NEMS transducer, measured thermomechanical noise with different resolution bandwidth (RBW), equivalent model parameters of AlN square membrane NEMS resonators, balanced bridge scheme to nullify background response, design of NEMS structure to achieve predictable threshold pump, and benchmarking force sensitivity in NEMS transducers.

We thank the financial support from the National Science Foundation (NSF) via CCF FET Program (Grant No. CCF 2103091). We thank Dr. M. H. Matheny, Professor M. L. Roukes, and Professor J. Lee for their generous support from previous collaborative projects and helpful discussions.

# AUTHOR DECLARATIONS Conflict of Interest

The authors have no conflicts to disclose.

### **Author Contributions**

**Tahmid Kaisar:** Conceptualization (supporting); Data curation (lead); Formal analysis (equal); Investigation (lead); Methodology (equal); Validation (equal); Writing – original draft (lead); Writing – review & editing (equal). **Philip X.-L. Feng:** Conceptualization (lead); Data curation (supporting); Formal analysis (equal); Funding acquisition (lead); Investigation (equal); Methodology (equal); Project administration (lead); Resources (lead); Supervision (lead); Validation (equal); Writing – original draft (equal); Writing – review & editing (equal).

### **DATA AVAILABILITY**

The data that support the findings of this study are available in supplementary material and from the corresponding author upon reasonable request.

### **REFERENCES**

- <sup>1</sup>K. L. Ekinci and M. L. Roukes, Rev. Sci. Instrum. 76, 061101 (2005).
- <sup>2</sup>Y. T. Yang, C. Callegari, X. L. Feng, K. L. Ekinci, and M. L. Roukes, Nano Lett. 6, 583 (2006).
- <sup>3</sup>X. L. Feng, C. J. White, A. Hajimiri, and M. L. Roukes, Nat. Nanotechnol. 3, 342 (2008).
- <sup>4</sup>X. M. H. Huang, X. L. Feng, C. A. Zorman, M. Mehregany, and M. L. Roukes, New J. Phys. 7, 247 (2005).
- <sup>5</sup>M. D. LaHaye, O. Buu, B. Camarota, and K. C. Schwab, Science **304**, 74 (2004).
- <sup>6</sup>D. S. Greywall, B. Yurke, P. A. Bush, A. N. Pargellis, and R. L. Willett, Phys. Rev. Lett. 72, 2992 (1994).
- <sup>7</sup>R. B. Karabalin, X. L. Feng, and M. L. Roukes, Nano Lett. **9**, 3116 (2009).
- <sup>8</sup>A. Eichler, J. Chaste, J. Moser, and A. Bachtold, Nano Lett. 11, 2699 (2011).
- <sup>9</sup>S. M. E. H. Yousuf, J. Lee, S. W. Shaw, and P. X.-L. Feng, J. Microelectromech. Syst. 32, 335–346 (2023).
- <sup>10</sup>R. B. Karabalin, S. C. Masmanidis, and M. L. Roukes, Appl. Phys. Lett. **97**, 183101 (2010).
- <sup>11</sup>J. Lee, C.-S. Li, Z. Wang, M.-H. Li, C.-H. Chin, S.-S. Li, and P. X.-L. Feng, in *IEEE International Frequency Control Symposium*, Taipei, Taiwan (IEEE, 2014), pp. 1–3.
- <sup>12</sup>J. M. L. Miller, A. Ansari, D. B. Heinz, Y. Chen, I. B. Flader, D. D. Shin, L. G. Villanueva, and T. W. Kenny, Appl. Phys. Rev. 5, 041307 (2018).

- <sup>13</sup>G. Parakash, S. Hu, A. Raman, and R. Reifenberger, Phys. Rev. B 79, 094304 (2009).
- <sup>14</sup>S. H. Nitzan, V. Zega, M. Li, C. H. Ahn, A. Corigliano, T. W. Kenny, and D. A. Horsley, Sci. Rep. 5, 9036 (2015).
- <sup>15</sup>L. G. Villanueva, R. B. Karabalin, M. H. Matheny, E. Kenig, M. C. Cross, and M. L. Roukes, Nano Lett. 11, 5054 (2011).
- <sup>16</sup>J. Lee, M. H. Matheny, M. L. Roukes, and P. X.-L. Feng, in *Proceedings of IEEE International Conference on Micro Electro Mechanical Systems*, Seoul, Korea (IEEE, 2019), pp. 879–882.
- <sup>17</sup>I. Mahboob and H. Yamaguchi, Nat. Nanotechnol. 3, 275 (2008).
- <sup>18</sup>J. Suh, M. D. LaHaye, P. M. Echternach, K. C. Schwab, and M. L. Roukes, Nano Lett. **10**, 3990 (2010).
- <sup>19</sup>P. Prasad, N. Arora, and A. K. Naik, Nanoscale 9, 18299 (2017).
- <sup>20</sup>R. Singh, R. J. T. Nicholl, K. I. Bolotin, and S. Ghosh, Nano Lett. **18**, 6719 (2018)
- <sup>21</sup>R. J. Dolleman, S. Houri, A. Chandrashekar, F. Alijani, H. S. J. van der Zant, and P. G. Steenken, Sci. Rep. 8, 9366 (2018).
- <sup>222</sup>J. Lee, S. W. Shaw, and P. X.-L. Feng, Appl. Phys. Rev. **9**, 011404 (2022).
- 23S. M. E. H. Yousuf, Y. Wang, J. Lee, S. W. Shaw, and P. X.-L. Feng, in Proceedings of IEEE International Conference on Micro Electro Mechanical Systems, Munich, Germany (IEEE, 2023), pp. 613–616.
- <sup>24</sup>O. Thomas, F. Mathieu, W. Mansfield, C. Huang, S. Trolier-McKinstry, and L. Nicu, Appl. Phys. Lett. **102**, 163504 (2013).
- 25D. Rugar and P. Grütter, Phys. Rev. Lett. **67**, 699 (1991).
- <sup>26</sup>I. Mahboob and H. Yamaguchi, Appl. Phys. Lett. **92**, 253109 (2008).
- <sup>27</sup>S. Wu, J. Sheng, X. Zhang, Y. Wu, and H. Wu, AIP Adv. 8, 015209 (2018).
- <sup>28</sup>T. Kaisar, J. Lee, D. Li, S. W. Shaw, and P. X.-L. Feng, Nano Lett. 22, 9831 (2022).
- <sup>29</sup>Y. Zhang, J. Moser, J. Güttinger, A. Bachtold, and M. I. Dykman, Phys. Rev. Lett. 113, 255502 (2014).
- <sup>30</sup>H. W. C. Postma, I. Kozinsky, A. Husain, and M. L. Roukes, Appl. Phys. Lett. 86, 223105 (2005).
- <sup>31</sup>J. Lee, Z. Wang, K. He, R. Yang, J. Shan, and P. X.-L. Feng, Sci. Adv. 4, eaao6653 (2018).
- 32T. Kaisar, S. M. E. H. Yousuf, J. Lee, A. Qamar, M. Rais-Zadeh, S. Mandal, and P. X.-L. Feng, IEEE Trans. Ultrason., Ferroelectr., Freq. Control 70, 1213 (2023)
- 33J. M. L. Miller, D. D. Shin, H.-K. Kwon, S. W. Shaw, and T. W. Kenny, Appl. Phys. Lett. 117, 033504 (2020).
- <sup>34</sup>T. D. Stowe, K. Yasumura, T. W. Kenny, D. Botkin, K. Wago, and D. Rugar, Appl. Phys. Lett. **71**, 288 (1997).